Variation of the Redox Conditions and the Resultant Phase Assemblages during Iron Ore Sintering

Teresa van den Berg
teresavdberg@gmail.com
Johan de Villiers (corresponding author)
johan.devilliers@up.ac.za
Robert Cromarty
robert.cromarty@up.ac.za
Department of Materials Science and Metallurgical Engineering
University of Pretoria
Pretoria 0002 South Africa

Highlights

- The oxygen potential in a sinter bed is measured by a zirconia oxygen probe to be ~ 0.01 atm.
- This oxygen potential in the sinter is appreciably more oxidizing than previous estimates.
- The contents of a quenched sinter pot show that at the flame front, only magnetite and slag are present.
- SFCA phases only form to a limited extent at the top of the quenched bed.
- Thermodynamic modeling at a pO_2 of 0.01 atm is in qualitative agreement with the phase analysis of the sinter pot.

Abstract

The oxygen potential prevailing during iron ore sintering was measured with a zirconia sensor in a series of sinter pot experiments. This was done to get a better indication of the redox conditions during commercial sintering. It was found that the pO_2 is appreciably more oxidizing than previously assumed, with a minimum value of ~0.01 atm. It is concluded that this value represents the oxygen potential of the gas phase and it is therefore a mixture of combustion gas and downdraft air.
The contents of a quenched sinter pot where the reactions were interrupted with the flame front situated midway through the sinter bed were investigated. X-ray diffraction analysis, using an internal standard to quantify the amorphous slag phase, revealed that at the flame front only magnetite and slag was present. SFCA phases only formed at the top of the bed after the flame front had passed. Thermodynamic modeling of the phases at equilibrium agree qualitatively with the phase analysis and explained the extensive presence of magnetite and melt, as well as the formation of calcium ferrite phases during cooling below 1100°C.

1. Introduction

The variation in redox conditions during iron ore sintering has been the subject of discussion in a number of publications. It is generally agreed that drying, dehydration, and carbonate dissociation

occur at the preheating zone ahead of solid fuel combustion. The sintering reactions are initiated at the flame front where the fuel (usually coke or char) is combusted. The flame front rapidly moves downward through the sinter bed by the suction of the combustion gas. At the combustion zone the redox conditions are reducing and this then changes to oxidizing as the already sintered material cools by the downward passage of air through the partially molten charge[1]. Eventually the sintering reaction stops at the grid layer, consisting of previously produced sinter, where the absence of fuel terminates the sintering reaction and the entire sinter bed cools as it moves down the sintering line.

Establishing the redox conditions during sintering was indirectly monitored by determining the CO and CO_2 contents in the off-gas (steady state waste gas composition, SSWGC) during sintering[2,3]. This is an average of all reactions taking place during sintering, reflecting both combustion and cooling conditions. It is however useful in monitoring coke additions to regulate the temperature during sintering.

To evaluate the reactions taking place during sintering, fine-grained synthetic mixtures were examined by in situ high-temperature X-ray diffraction in air and at slightly reducing conditions[4,5,6] using laboratory and synchrotron sources. These studies, although not quite representing actual sintering conditions, are valuable in that they established the temperature conditions where the major phases magnetite, hematite and the silico-ferrite binding phases, SFCA (silico ferrite of calcium and aluminium)and SFCA-I, form. These phases will be discussed in more detail later.

The melting behavior of $CaO\text{-}SiO_2\text{-}FeO_x$ slags were investigated at various oxygen partial pressures using chemical equilibration and optical microscopy and the phase relations were established[1,7]. This is of importance because of the wide range of pO_2 conditions encountered during sintering. These conditions were simulated in laboratory tests at various temperatures and redox conditions during heating and cooling.

In addition, some studies on larger sinter pot samples where the flame was terminated by the introduction of nitrogen[8,9] was done to study reactions before, during and after ignition. These studies are important in that sinter reactions can be terminated at positions at the flame front and also below and above this zone.

The phase relations and melting behaviour of sinters were investigated by Kongoli et al.[10] and they have published liquidus surfaces at various pO_2 values and with various basicities, MgO and Al_2O_3 contents.

The aims of the present investigation are the following: (1) the direct measurement of the pO_2 while the flame front moves past the probe and (2) a separate investigation of phase formation in sinter pots that were quenched with liquid nitrogen or water. The latter study investigated phase relations that form ahead of the flame front during heating, at the front during combustion, and behind the front during air cooling. (3) Thermodynamic modeling was performed to explain the presence of magnetite and to determine the solidus temperature.

2. Materials and methods

2.1. Pot test experiments

A split circular pot (internal diameter 20 cm) of 40 cm height was used in the tests. The two halves of the pot were clamped tightly and sealed with clay to prevent leakage. Thermocouples were inserted at three locations as shown in Figure 1.

Figure 1: Test pot used in the experiments. Thermocouple 1 is at the top, Thermocouple 2 in the middle and thermocouple 3 is at the bottom. The diameter is 200mm and the height 400mm.

The pot was ignited using gas burners at the top of the pot and suction was applied from the bottom. When the middle thermocouple showed maximum temperature the aim was to "freeze" the pot in order to stop all reactions taking place. In the first experiment liquid nitrogen was poured on top of the sinter pot. In the second experiment water was used. Air suction was not stopped during the cooling of the pot test in order to promote the cooling effect through the sinter material. The pot was then opened and the top layer of material was removed. The samples were then collected from the centre section of the pot since this area is not associated with shrinkage due to the inflow of excess air or because edges of the pot might not receive sufficient heat and therefore result in incomplete sintering.

The following sinter parameters were used for all experiments:

Bed height	400mm
Ignition temperature	1058°C
Pressure drop	1000 mm H_2O
Fuel addition	4.7%

2.2. Sinter composition

The composition of the sinter is given in Table 1. Return fines were omitted on purpose so as to establish the reactions that the mix undergoes without contaminating it with previously reacted material. The elevated MgO content was chosen to evaluate the deleterious effect when dolomite is used to substitute for calcite[11]. LOI was determined gravimetrically on the material after the completed sinter test.

Table 1. Composition of the sinter mix used in this study

Fe(tot)	FeO	Fe2O3	CaO	MgO	SiO2	Al2O3	K2O	Na2O	TiO2	MnO
55.10	9.17	68.60	10.30	3.03	5.79	1.69	0.229	0.079	0.132	0.824
P	**S**	**C**	**LOI**	**Basicity**						
0.063	0.013	0.027	-0.880	1.78						

2.3. pO_2 measurements as a function of temperature

$SIRO_2$ C700+ oxygen sensors[12] were used in all the pO_2 tests performed. The sensor is a solid electrolyte oxygen concentration cell developed by the Division of Material Science, CSIRO, Australia to enable in-situ measurements of the oxygen content or the equilibrium oxygen partial pressure in gas mixtures above 700°C. The sensor consists of an impervious alumina tube containing a zirconium oxide-based pellet at one end (Figure 2). The protruding part of the pellet is coated with porous platinum and carries circumferential grooves to facilitate the attachment of a wire lead to the external electrode. The pellet end inside the sensor is also coated with porous platinum. The zirconia-based pellet in the sensor is an oxygen ion-conducting solid-electrolyte.

When there is an oxygen concentration gradient across the sensor an emf (E), which obeys the Nernst equation develops. If air is used as a reference the oxygen partial pressure can be calculated from the EMF and absolute temperature using the following equation:

$$pO_2 = 0.209 \exp(-46.421\ E/T)$$

where E is the measured Voltage and T the temperature in Kelvin.

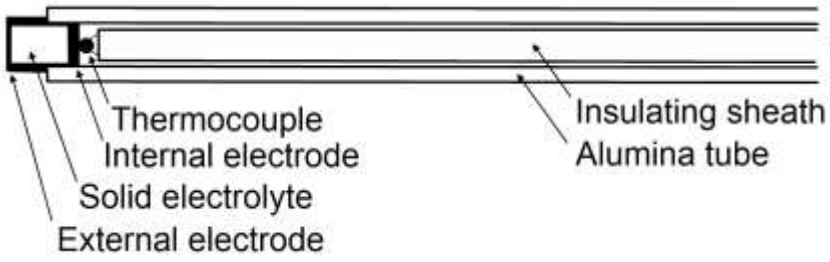

Figure 2: The $SIRO_2$ sensor

The oxygen sensors are accurate between 700 – 1700°C.

The sensors were calibrated in the laboratory according to the following method. A mullite tube was partially inserted into a small tube furnace. The oxygen sensor was then inserted into this tube with a gas inlet on the opposite end. Inside the oxygen sensor an S-type thermocouple was inserted. A tube was fitted over the end of the oxygen sensor and thermocouple. This tube was then connected to a small compressor pump. The oxygen sensor has a Pt-coated electrode which is connected to the data logger with a pure Pt-wire. The data logger was connected to a computer and was set to measure the voltage and temperature every second. Calibration tests were carried out at temperatures between 700 - 1300°C.

The sensors were first calibrated using a gas mixture consisting of a 50% CO, 50% CO_2 using air as the reference. Over a measurement period of 1 hour and 34 minutes (1586 measurements) the average temperature was 809.9°C and the average measured log pO_2 was -18.12. According to the tables of Deines et al[13] at 810°C, for a 50:50 CO-CO_2 mixture, log pO_2 is -18.15. The corresponding value calculated by FACTsage is -18.08. This indicates a good correspondence between the sensor and calculated values.

Initially the sensor was inserted horizontally in a sinter pot together with three additional thermocouples. When the sinter mixture was combusted, shrinkage of the sinter mixture caused the connecting alumina tube to break. This caused several experiments to fail. The experiments were then repeated with the probe tube almost vertical. This arrangement allowed uninterrupted measurements to be conducted. Most experiments were done with the sensor in the middle of the sinter pot. The arrangement is shown in Figure 3. All measurements were done on the same sinter mixture and are essentially repeats of the same experiment.

Using this procedure, it is clear that an average pO_2 is being measured as the flame proceeds through the sinter bed. Locally, the value can be far lower in the vicinity of coke or fuel particles. This also explains the variability of the measurements due to the position of the sensor in relation to fuel particles.

Figure 3. Location of the oxygen sensor in the sinter pot

2.4. Phase characterization of the quenched sinter

In order to study the reactions taking place at the various zones of the sinter bed, the bed was quenched with liquid nitrogen or with water when the flame front showed a maximum temperature at the middle thermocouple. The temperature profiles during liquid nitrogen and water quenching are shown in Figure 4. Judging from the temperature profiles during quenching, the water quench was the most successful in cooling the sinter bed. This is evident in comparing the cooling of the pots after quenching. The pot cooled by liquid nitrogen did not cool down sufficiently fast as shown by the temperature profiles of the middle and bottom thermocouples. This is probably due to insufficient contact between the liquid nitrogen and the hot sinter. Conversely, the middle and bottom thermocouples of the water cooled pot show fast cooling after quenching. The high thermal conductivity and high heat of vaporization and high boiling point of water make it an extremely effective quench medium. Due to the rapid cooling water quenched pots would better reflect sintering conditions prevailing at the time of the quench.

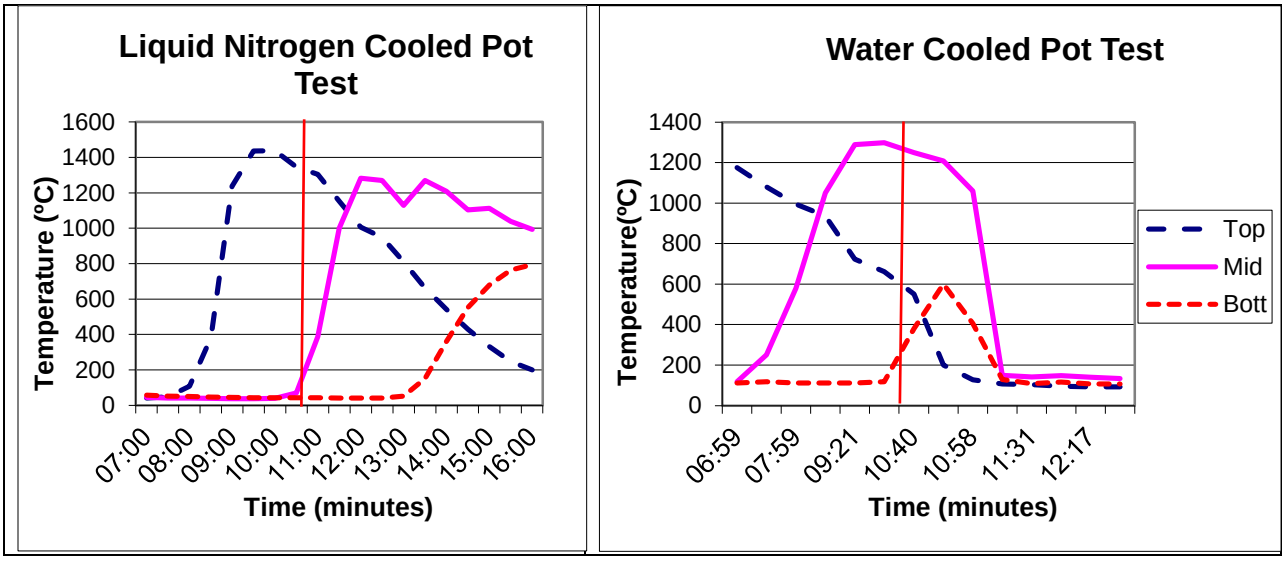

Figure 4. Temperature profiles of the top, middle and bottom thermocouples for the liquid nitrogen and water quenched sinter pot tests. The red vertical lines show when the quenching commenced. Quenching is less effective for the nitrogen cooled test than for the water cooled test.

The sinter pot was split open and samples taken at regular intervals, as shown in Figure 5.

Figure 5. Sample locations in the water quenched sinter pot, labeled from top (1) to bottom (8). Sample 7 and 8 consist of the grid layer of previously sintered material.

2.5 XRD Analysis

These samples were milled, micronized, and mixed with a silicon internal standard so that the amount of quenched slag can be quantified in addition to the crystalline phases.

A PANalytical X'Pert Pro powder diffractometer with X'Celerator detector and variable divergence- and receiving slits with Fe filtered Co Kα radiation was used for data collection.

Phase quantification was done using the Rietveld method using the Autoquan program[14]. Crystal structure data of the crystalline phases and silicon standard were obtained from the ICSD crystal structure data base, with the exception of the SFCA structure, which was determined separately[15]. The crystal structure data are then used to calculate XRD patterns that are fitted to the experimental patterns. In general the fits are quite good with average errors in quantification of <2% for the major phases magnetite, hematite, SFCA and SFCA-I. For the quantification of the slag phase 20% of a silicon internal standard was mixed with each sinter sample.

The SFCA phases are the important binding phases in iron ore sinters and they belong to the aenigmatite structure type with SFCA having a $M_{14}O_{20}$ stoichiometry and SFCA-I being closely related to SFCA with a $M_{20}O_{28}$ stoichiometry (M denoting the sum of all cations). The two phases belong to a homologous series of compounds with formula $M_{14+6n}O_{20+8n}$ with n=0 and 1 respectively[16].

2.4 SEM analysis of the melt phase

The melt phase in four samples were analysed on polished sections of the powdered samples using a JEOL JSM IT300 electron microscope operated at 15kV. Standard ZAF corrections were made using the Oxford Instruments XMAX50 software. The compositions are expressed as percentages of the oxide components.

2.5 Thermodynamic analysis

Thermodynamic modeling was performed using the FACTSage™ software[17], similar to the method used by Xuewei et al[18]. The Equilib option was used with the composition as given in Table 1. Phases that were used are FToxid-SLAGA, FToxid-SPINA, FToxid-CORU, FToxid-MeO_A, FToxid-aC2S, FToxid-bC2S. As there is no data available for SFCA, the phase FToxid-CAF2 was chosen as being closest in

composition to SFCA. The equilibrium phase assemblages were calculated at a fixed pO_2 of 0.01 atm every 100°C between 500°C and 1500°C. Compositions of the various phases, including the liquid phase were also calculated

3. Results

3.1. pO2 measurements

The results of the pO_2 measurements are summarized in Figure 6.

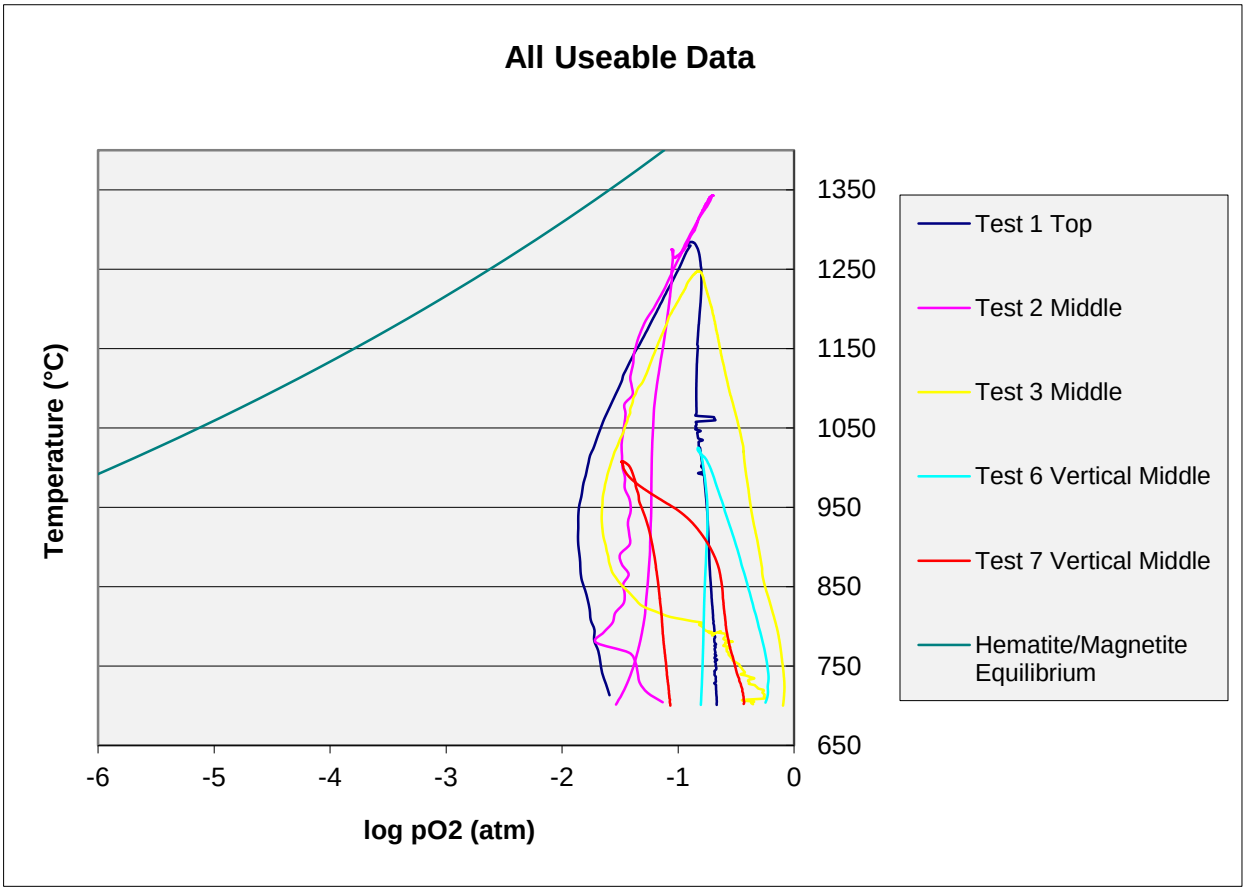

Figure 6. Variation in pO2 and temperature as the sinter bed was heated and cooled. The pO_2 is first decreased as the temperature increases due to combustion and then increases during air cooling. The legend gives the location of the sensor in the sinter pot. Tests 6 and 7 were conducted with the sensor in the almost vertical orientation.

As can be seen from the figure, the results are highly variable, but all follow the same expected trend, i.e. a decrease in pO_2 with increasing temperature, followed by an increase during cooling by the downdraft air. The reason for this variability is most likely due to the non-homogeneity of the sinter bed, the proximity of char to the sensor and the variability of gas movement through the permeable sinter bed. Surprisingly, the log pO_2 does not decrease below -2, and this seems to argue against the predominance of magnetite in most sinters, but its presence is predicted by the FACTsage modeling.

3.2 Phase quantification

The distribution of the different phases as a function of bed height is shown in Table 2 and on Figure 7. Sample 1 is at the top and 6 at the bottom of the bed. Errors in phase quantities vary from 0.5% for the crystalline phases and 1.5% for the slag phase.

Table 2. Variation in phase quantities in the quenched sinter bed samples (mass%).

	WNRF1	WNRF2	WNRF3	WNRF4	WNRF5	WNRF6
Amorphous(slag)	18.77	28.68	52.27	33.17	36.23	6.41
C2S beta	5.31	1.39	2.87	6.42	4.75	1.7
Calcite	1.28	0.75	1.15	0.99	0.53	5.84
Dolomite	0.23	0.17	0.15	0.46	0.12	4.63
Hematite	19.86	17.38	9.23	5.44	7.54	67.75
Magnetite	39.51	48.57	30.38	44.88	40.46	8.56
Quartz	0.65	0.51	0.57	0.29	0.5	3.83
SFCA1	3.38	0	1.04	1.71	1.95	0.74
SFCA	10.04	2.43	2.34	1.09	1.87	0.49
Wuestite	0.97	0.12	0	5.54	6.07	0.05

Several aspects are noteworthy; first, there is still unreacted calcite, dolomite and quartz and predominant hematite in the bottom sample - an indication that the flame front is not yet affecting the bottom of the quenched bed. Also of interest is the presence of small amounts of wüstite in samples 4 and 5. Wüstite was also found to be present in quenched sinter samples by Choudhary[8]. The maximum amount of melt is present in sample 3, presumably at the flame front. Also of significance are the very small amounts of SFCA and SFCA-I in samples 2 to 6, as compared to the amounts of SFCA and SFCA-I in commercial sinters. This is a strong indication that the SFCA phases form during cooling of the sinter bed, after the formation of magnetite. This is confirmation of the findings of Webster et al.[5] who found that SFCA forms after melting and magnetite crystallization. However, no evidence could be found for the solid state formation of SFCA species during heating below the melting temperature, but this could be due to the sharp temperature gradient between samples 5 and 6; significant melting has already started in sample 5 with 36% melt. On the other hand, the presence of unreacted calcite and dolomite is an indication that the sample is below the formation temperature of the SFCA phases.

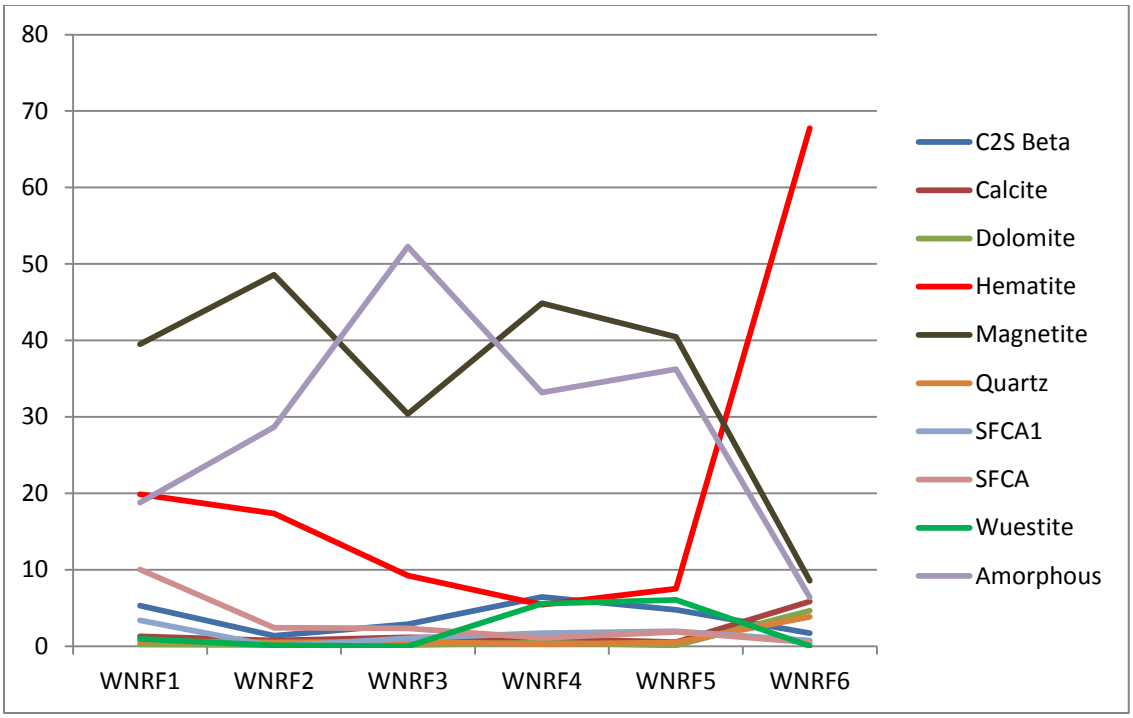

Figure 7. Distribution of the phases in the water quenched sinter pot samples as mass percentages. Sample 1 is at the top of the sinter bed and sample 6 at the bottom. The flame front is situated at the position of sample 3.

3.3 Liquid composition

The composition of the liquid phase (given as mass fractions), the amount of slag and the slag basicity as a function of temperature, calculated by FACTsage, is given in Table 3, and in Figure 8.

Table 3. Composition of the liquid phase amount of slag and slag basicity upon cooling

	Temperature -°C				
Mass Fraction	1100	1200	1300	1400	1500
K2O	0.001	0.042	0.006	0.004	0.003
Al2O3	0.108	0.057	0.023	0.019	0.017
SiO2	0.001	0.291	0.143	0.109	0.067
CaO	0.161	0.392	0.255	0.194	0.119
FeO	0.003	0.015	0.060	0.114	0.201
Fe2O3	0.705	0.175	0.487	0.532	0.558
MgO	0.002	0.008	0.006	0.012	0.026
MnO	0.000	0.017	0.012	0.009	0.005
Mn2O3	0.019	0.003	0.009	0.007	0.004
TOTAL:	1.000	1.000	1.000	1.000	1.000
Gram Slag	0.802	5.218	40.466	53.226	86.671
Basicity	161	1.3	1.8	1.8	1.8

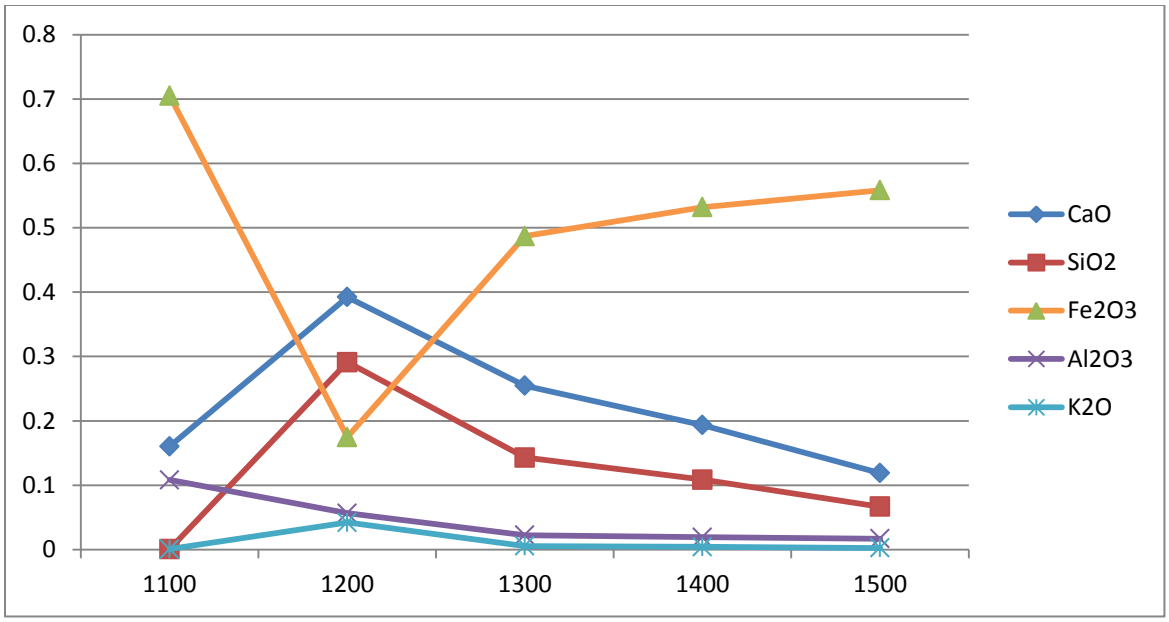

Figure 8. Calculated slag compositions as a function of temperature

From the data it is apparent that the Fe_2O_3 content of the slag phase gradually decreases with a decrease in temperature whilst the CaO, SiO_2 and Al_2O_3 contents increase. The values at 1100°C are atypical since there is only 0.8% melt left.

The average slag compositions for four analysed WNRF samples are remarkably constant and do not show the expected compositions as shown in Figure 8. The compositions of the major components of four samples are shown in Figure 9. These compositions are closest to the calculated ones at 1200°C. The most probable reason for this finding is that the liquid phase in all the samples had enough time to re-equilibrate to a constant composition during the time that it cooled.

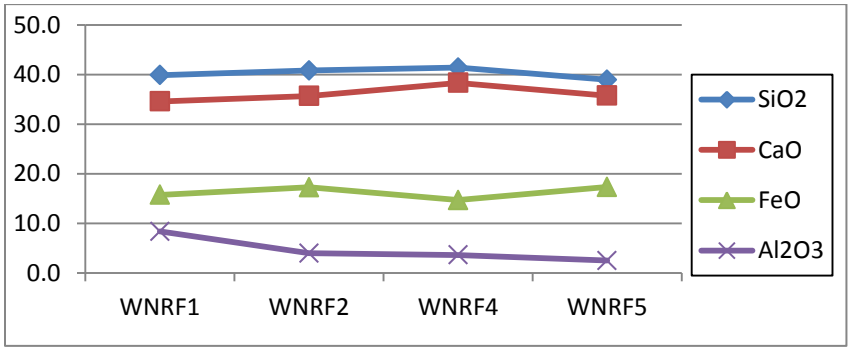

Figure 9. Average slag compositions of the samples as indicated. These are remarkably constant and within the error limits as determined by the individual slag analyses.

4. Discussion

4.1. pO_2 measurements

Comparison with estimates from the literature show that the measured values from this study are much more oxidizing than those given by Hsieh and Whiteman[1], (log pO_2 of 10^{-2} measured compared to 10^{-9} during heating and 0.21 atm during cooling[1]). They reported that at a pO_2 value of 5×10^{-3} atm the mixture consists of 48 percent magnetite, 31 percent calcium ferrite, and 21 percent glass or slag.

Kongoli *et. al.* [10] have estimated the oxygen potential during sintering and have concluded that it is scattered from 10^{-12} to10^{-4} atm as a result of various short time heterogeneous reactions. It depends on several factors such as the layer, temperature, coke size, its amount, etc. Nonetheless they suggest that the normal oxygen potential during sintering can vary from 10^{-6} to 10^{-7} atm.

The pO_2 values reported here are considered accurate, but the sensor probably measures the value for the gas phase that is a mixture of the combustion gas mixed with the cooling downdraft air. On the other hand, it might be expected that the phase assemblage might differ depending on whether the sinter mix is in contact with char or not.

Comparison with the hematite-magnetite equilibrium shows that the measured pO_2 is more oxidizing, and therefore the presence of predominant magnetite needs an explanation.

Simulation of the phase equilibria using FACTSage™was attempted using the analyzed sinter composition and a gas mixture approximating the measured pO_2. The maximum temperature was taken as 1500°C and the log pO_2 kept at -2. Cooling was simulated by decreasing the temperature by 100 degrees per step, keeping the pO_2 constant at 0.01 atm. This is shown in Figure 10.

Unfortunately, there is no thermodynamic data available for the SFCA phases, and they will be approximated by calcium ferrite that contains no silica. The stable calcium ferrite is calculated to be $CaFe_2O_4$, which was not observed in the samples investigated. This is probably due to the absence of thermodynamic data for the SFCA phases. Nevertheless $CaFe_2O_4$ was reported as an intermediate phase (event 5) by Webster et al.[5].

Comparison with the phase quantities as reported by Hsieh and Whiteman[1] at a pO_2 of 5×10^{-2} with rapid cooling show the following approximate contents of the major phases: hematite, 21%; magnetite, 40%; calcium ferrite, 13%; and slag, 24%. This is in agreement with sample WNRF1 at the top of the sinter bed.

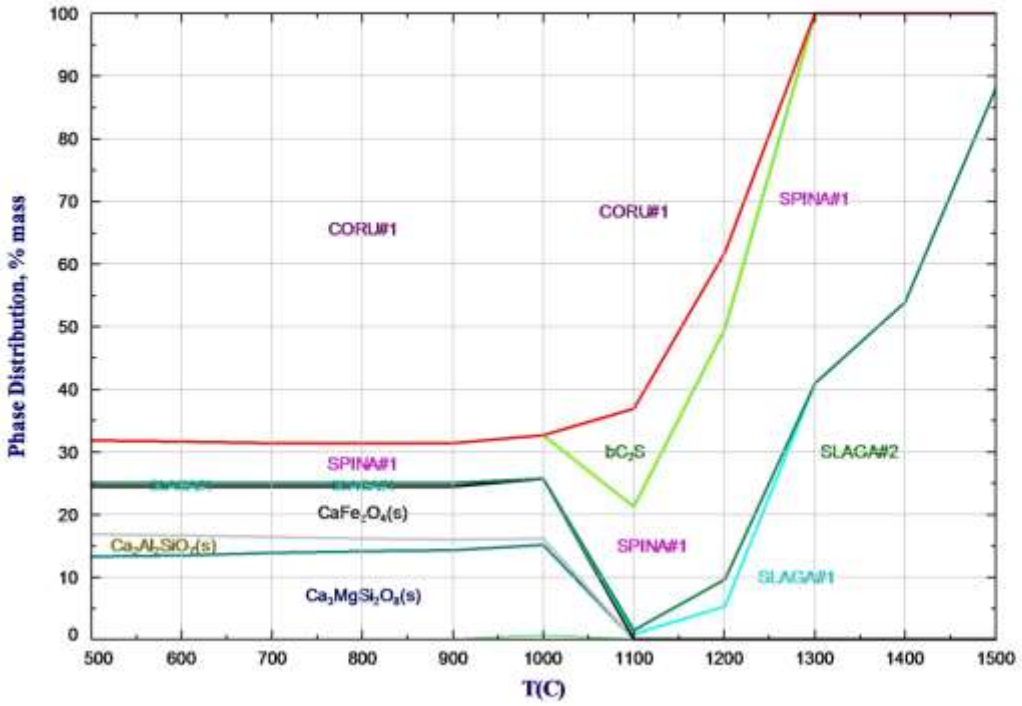

Figure 10. Phase distribution of a sinter of composition as in Table 1 as a function of temperature.. Magnetite is represented as SPINA#1, hematite as CORU#1 and slag as SLAGA#1.

The predominance of magnetite plus slag is clearly shown at 1300°C, and the solidus temperature is 1100°C. Also apparent is the formation of calcium ferrite only after the disappearance of slag.
An important conclusion from this calculation is the fact that the major SFCA binding phases are formed only on cooling, and that the extent of melt formation together with the cooling history of the sinter are most probably major factors affecting the properties of the sinter.
Comparison of the FACTsage results with the phase quantities determined by XRD below the solidus temperature of ~1100°C cannot be done because of the absence of SFCA in the database. This leads to the calculated stability of other phases (merwinite and Ca ferrite) that obviously are absent. However, the calculated phase quantities above the solidus temperature are in qualitative agreement with the observed phase quantities.

4.2 Phase characterization

Examination of the phase assemblages of the quenched samples shows that at the flame front, (Sample WNRF3), the major phases are magnetite and melt, with minor (relict?) hematite. This is qualitatively in agreement with the thermodynamic modeling and with the findings of Webster et al[5].

Melt compositions as measured by SEM analysis show that their compositions are very similar and this probably reflects a melt composition quenched at 1200°C, when compared with compositions calculated by thermodynamic modeling.
The SFCA phases are not stable in the presence of melt; this was conclusively shown by Webster et al[5]. This is confirmed by this study, as can be seen in Table 2, and in Figure 5. They only start to appear at the top of the bed. This has important implications for sinter formation. It is clear therefore that the sinter assemblage is formed during cooling and after crystallization of the slag phase. This means that sinter strength is mainly developed during cooling with the crystallization of the SFCA phases. Magnetite is a residual phase preserved from the reaction in the flame front and hematite can either be a relict phase or it can form from the melt.
The measured compositions of the liquid phase in all the samples from the quenched sinter pot are remarkably constant and most probably reflect a composition where crystallisation of the solid phases ceased, leaving a residual quenched slag phase.
More attention needs to be given to reactions that take place during cooling of the bed, as this can maximise SFCA formation, the main binding phases in the sinter. The combustion step, important for the development of sufficient melt formation, assumes less importance for the development of strong sinter.

5. Conclusions

This study has shown that the pO2 developed during sintering, as measured by a zirconia oxygen sensor, is significantly more oxidizing than previously postulated, with a minimum value of ~0.01 atm at a temperature of 1300°C.

Examination of samples from a quenched sinter pot show magnetite plus melt as the major phases at the flame front, with essentially no development of SFCA phases. These phases only form when the melt phase is greatly diminished.

Thermodynamic modeling keeping the pO2 at 0.01 atm. is in qualitative agreement with the phase analysis of the quenched sinter samples, and with the findings of Hsieh and Whiteman[1] and Webster et al[5].

More attention should be given to the quenching part of the sinter operation since this is where the SFCA binding phases form. Changing cooling rates by control of incoming air temperatures could enhance or inhibit the formation of these phases with a concomitant change in the metallurgical properties such as tumble index or reduction disintegration index.

6. Acknowledgments

The assistance of Andre Dippenaar and Kobus Vreugdenburg from Anglo American Kumba for pot sinter tests is acknowledged. These were conducted in addition to their normal duties. They also provided valuable input to make these tests a success. The first author also acknowledges financial assistance from Kumba in the form of a bursary.

Thanks also to Johan Zietsman for assistance with the FACTsage modeling and for valuable suggestions. The comments of Andrie Garbers-Craig are also gratefully acknowledged.

7. References

1. Hsieh, L and Whiteman, J A, Sintering Conditions for Simulating the Formation of Mineral Phases in Industrial lron Ore Sinter, ISIJ International, Vol. 29 (1989), pp 24-32.
2. Zhou,H, Zhao,J P, Loo, C E, Ellis, B G and Cen, K F, Model Predictions of Important Bed and Gas Properties during Iron Ore Sintering, ISIJ International, Vol. 52 (2012), No. 12, pp. 2168–2176
3. Loo, C E, Tame, N and Penny, GC, Effect of Iron Ores and Sintering Conditions on Flame Front Properties, ISIJ International, Vol. 52 (2012), No. 6, pp. 967–976
4. Scarlett, N V Y, Madsen, I C, Pownceby, M I and Christensen, A, N. Reaction sequences in the formation of silico-ferrites of calcium and aluminium in iron ore sinter. Metallurgical and Materials Transactions B, Vol 35B (5), pp. 929-936
5. Webster, N A S, Pownceby, M I, Madsen, I C and Kimpton, J A, Silico-ferrite of calcium and aluminum (SFCA) iron ore sinter bonding phases: new insights into their formation during heating and cooling. Metallurgical and Materials Transactions B, (2012) Vol. 43B, pp. 1346-1357
6. Webster, N A S, Pownceby, M I and Madsen, Effect of oxygen partial pressure on the formation mechanisms of complex Ca-rich ferrites, ISIJ International, Vol. 53 (2013), No. 8, pp. 1334–1340
7. Matsuura, H, Kurashige, M, Naka, M and Tsukihashi, F, Melting and solidifying behaviors of the CaO–SiO2–FeOx slags at various oxygen partial pressures, ISIJ International, Vol. 49 (2009), No. 9, pp. 1283–1289
8. Choudhari, M J, Evolution of Sinter Structure along Bed Height of quenched Test Pot, ISIJ International, Vol. 47 (2007), No. 3, pp. 516–518
9. Choudhary, M K, Bhattacharjee, D, Bannerjee, P S, and A. K. Lahiri, A K, Effect of variation of alumina on development of phases during iron ore sintering, ISIJ International, Vol. 48 (2008), No. 12, pp. 1804–1806
10. Kongoli F, McBow, I, Budd R, Llubani, S and Yazawa, A, Effect of oxygen potential and fluxing components on phase relations during sintering of iron ore, J. Min. Metall. Sect. B-Metall. Vol. 46 B (2), 2010 pp.123 – 130
11. Panigrahi, S C, Rigaud, M and Dilewijns, J, Effects of replacement of limestone by dolomite and other MgO materials on production rate of iron ore sinter, Ironmaking and steelmaking, Vol 11 (5) 1984 pp 246-252
12. http://www.cof.com.au/nernst.shtml/
13. Deines, P, Nafziger, R H, Ulmer, G C and Woermann, E. Temperature-oxygen fugacity tables for selected gas mixtures in the system C-H-O at one atmosphere total pressure, Bulletin of the Earth and Mineral Sciences Experiment Station, 88, (1974) The Pennsylvania State University
14. Kleeberg, R, Bergmann, J, Quantitative phase analysis using the Rietveld method and a fundamental parameter approach, In: Sengupta, S P , Chatterjee, P (Eds.), Powder Diffraction: Proceedings Second International School on Powder Diffraction, 2002 pp. 63–67
15. Liles, D C, de Villiers, J P R and Kahlenberg, V, Refinement of iron ore sinter phases: a silico-ferrite of calcium and aluminium (SFCA) and an Al-free SFC, and the effect on phase quantification by X-ray diffraction, Mineralogy and Petrology, (2015) DOI 10.1007/s00710-015-0411-5
16. Mumme, W G, Clout, J M F, and Gable, R W, The crystal structure of SFCA-I, a homologue of the aenigmatite structure type, and new crystal structure refinements of β-CFF, and Mg-free SFCA, N. Jb. Min. Abh. Vol. 173(1) 1998 pp. 93-117
17. http://www.factsage.com/
18. Xuewei LV, Chenguang BAI, Qingyu DENG, Xiaobo H and Guibao QIU, Behavior of liquid phase formation during iron ores sintering, ISIJ International, Vol. 51 (2011), No. 5, pp. 722–727